https://doi.org/10.37434/tpwj2021.06.05

INVESTIGATION OF THE PRESENCE OF Mn^{4+} IN WELDING AEROSOLS USING RFS METHOD

O.M. Korduban[1], **V.V. Trachevskyi**[2], **T.V. Kryshchuk**[1], **I.R. Yavdoshchyn**[3] and **V.V. Holovko**[3]
[1]V.I. Vernadsky Institute of General and Inorganic Chemistry of the NAS of Ukraine
33/34 Palladin Prosp., 03142, Kyiv, Ukraine
[2]Technical Center of the NAS of Ukraine
13 Pokrovska Str., 04070, Kyiv, Ukraine
[3]E.O. Paton Electric Welding Institute of the NAS of Ukraine
11 Kazymyr Malevych Str., 03150, Kyiv, Ukraine. E-mail: office@paton.kiev.ua

Toxicity of welding aerosol significantly affects the choice of the type of electrodes for arc welding. Modern research methods allow determining the content of divalent and trivalent manganese particles in the solid component of welding aerosol. Studies were carried out to determine the ability of detecting the presence of ions in the most toxic tetravalent manganese in the solid component of welding aerosol. The possibility of using the method of RFS analysis for fixing manganese ions in the Mn^{4+} state in welding aerosols is shown. 9 Ref., 3 Tables, 2 Figures.

Keywords: welding, electrodes, aerosol, toxicity, manganese, X-ray fluorescence spectra

Arc welding processes are accompanied by high-temperature heating and evaporation of part of the base and electrode material, as well as slag which forms at electrode coating melting, flux-cored wire core or flux. Scattering of the formed gas-vapour mixture results in condensation of the vapour phase from the high-temperature zone of the arc discharge into the lower-temperature environment with formation of fine hard particles, suspended in the gas flow. This mixture of gases and fine hard particles forms the welding aerosol.

Welding aerosol contains toxic compounds harmful for the human body. Aerosol toxicity is related to the fact that the size of the majority of hard particles in its composition is less than 1 μm. The action of electrostatic and adsorption forces results in the hard aerosol particles forming agglomerates, the linear size of which varies in the range of 1–3 μm. Dimensions of individual particles change in the range from hundredth to tenth fractions of a micrometer. Larger particles of 1–2 μm size agglomerate, and finer ones form chains. Most of the fine particles have a nugget and shell. The nugget is enriched in iron and manganese compounds, and the shell contains silicon, potassium and sodium compounds. The shell thickness depends on temperature and oxidizing potential of the arc atmosphere, and it grows with increase of potassium and sodium content in the electrode coating. The structure heterogeneity is characteristic for condensation aerosols of a complex composition, which include aerosols forming in coated-electrode welding [1].

Manganese compounds are particularly dangerous from the viewpoint of toxicity. Toxicity of manganese compounds becomes higher with increase of its valence. Numerous studies of welding aerosols show that Mn is in Mn^{2+} and Mn^{3+} valent state [2]. Investigations conducted at PWI in recent years showed that manganese can be in the most toxic form of Mn^{4+} in the welding aerosol solid component (SCWA). Determination of the presence of such manganese in welding aerosol involves considerable difficulties, because of absence of reliable methods of analysis. In order to check the presence of Mn^{4+} states in the composition of welding aerosol (X-ray fluorescence spectroscopy), we studied the applicability of RFS analysis method.

Experimental procedure. In order to conduct the experiment, we prepared samples of aerosols, forming in welding with electrodes with different coating types, namely: acid (TsM-7), rutile (MR-3) and basic (UONI-13/55).

Electron structure of the samples surface was studied by RFS method in electron spectrometer with PHOIBOS-100 SPECS energy analyzer. The radiation source was an X-ray gun with magnesium anode (E MgK_α = 1253.6 eV, P = 300 W). Spectrometer calibration was performed in three points of energy scale by the position of maximums of $Au4f_{7/2}$–$Ag3d_{5/2}$- and $Cu2p_{3/2}$-lines. The values of E_b $Au4f_{7/2}$ = 84.0 eV, E_b $Ag3d_{5/2}$, and E_b $Cu3d_{5/2}$ = 932.6 eV were obtained that

V.V. Holovko — https://orcid.org/0000-0002-2117-0864

correspond to standard values of bond energy (E_b) [3]. Absolute separation, measured by $Au4f_{7/2}$- line of gold was equal to 0.9 eV, accuracy of determination of the position of $Au4f_{7/2}$-line maximum was ±0.05 eV.

Charging of the sample surface was taken into account by two methods. When allowing for the charge, the obtained values were recalculated to E_b C1s = = 285.0 eV and were compared with E_b obtained after neutralizing the surface charge, using slow electron gun FG 15/40. Working vacuum in the spectrometer analytical chamber was equal to $2 \cdot 10^{-7}$ Pa. Samples were prepared by applying aerogel in a mixture with hexan on copper substrates of 10×10 mm size.

Publications analysis shows that determination of the charge condition of manganese atoms by RFS method is not a trivial task even in simple systems.

In keeping with published data [4], E_b of maximums of $Mn2p_{3/2}$-line for Mn^{2+}-, Mn^{3+}- and Mn^{4+}-states in simple oxides changes in the following ranges: 640.4–641.0, 641.7–641.9 and 641.9–642.6 eV, respectively. However, decomposition of $Mn2p_{3/2}$-spectra of complex oxides into lines with such energies can be not quite correct. It is necessary to take into account the satellite contributions from each of these lines, which exactly lead to increase of the width and degree of asymmetry of Mn2p-spectra. However, it leads to subjective decisions without availability of sufficient criteria.

Another method to determine the charge state of manganese atoms is measurement of the difference in bond energies of $Mn2p_{3/2}$- and O1s-levels. In complex oxides, however, to which the studied samples belong, O1s-level is a superposition of the contributions of O1s-levels from oxides of several elements, while $Mn2p_{3/2}$-level also has several non-equivalent states that makes it practically impossible to single out E_b values, which are correlated with appropriate fragments of Mn^{n+}–O^{2-} bonds of manganese oxide lattice.

One more of these methods is analysis of the change of the width of Mn3s-spectra as a result of the exchange splitting. However, in the case of simultaneous existence, for instance, of contributions of Mn^{2+}- and Mn^{4+}-states the result will be averaged.

Thus, correct is the approach allowing for satellite contributions of Mn2p-lines. It consists in decomposition of $Mn2p_{3/2}$-spectra into the main line together with a group of its satellites, the parameters of which were obtained from calculation of photon-electron and electron-electron interaction [3].

Allowing for reaction kinetics at formation of iron-manganese aerosols indicates priority formation of oxide phases of iron and manganese, so that it is possible to apply the calculation results [3] for simple manganese oxides. According to calculations, the main Mn^{2+}–Mn^{3+} and Mn^{4+} lines in MnO, Mn_2O_3 and MnO_2 are accompanied by appearance of satellite lines, which are strictly deterministic by intensity I_{cat} and position ΔE relative to the main line.

Table 1. Bond energy and spectrum intensity

$Mn2p_{3/2}$	E_b, eV	I
Mn^{2+}	639.8	1.0
Mn^{2+}	641	0.71
Mn^{2+}	641.8	0.42
Mn^{2+}	642.7	0.3
Mn^{2+}	644.2	0.3
Mn^{3+}	640.7	1.0
Mn^{3+}	641.4	1.0
Mn^{3+}	642.2	1.16
Mn^{3+}	643.2	0.73
Mn^{3+}	644.6	0.28
Mn^{4+}	641.9	1.0
Mn^{4+}	642.9	0.65
Mn^{4+}	643.8	0.32
Mn^{4+}	644.8	0.1
Mn^{4+}	645.8	0.06
Mn^{2+}–F	640.2	1.0
Mn^{2+}–F	641.4	0.71
Mn^{2+}–F	642.2	0.42
Mn^{2+}–F	643.1	0.3
Mn^{2+}–F	644.6	0.3
Mn^{2+}–F	642.2	1.0
Mn^{2+}–F	643.4	0.71
Mn^{2+}–F	644.2	0.42
Mn^{2+}–F	645.1	0.3
Mn^{2+}–F	646.6	0.3

Using the results of work [3], $Mn2p_{3/2}$-spectra were decomposed into groups of five components, related to each other by energy and intensity (Table 1), after sequential allowing for the linear background and nonlinear background by Shirley method [5] and $K\alpha_{3,4}$, contributions from $Mn2p_{1/2}$-line (Table 1).

In the case of UONI 13/55 samples, the contribution of Auger-line of fluorine which was determined by the line from Caf_2 was subtracted from $Mn2p_{3/2}$-spectra. Table 1 gives the parameters for oxides with Mn^{2+}-, Mn^{3+}- and Mn^{4+}-states [3]. E_b values for two types of Mn^{2+}-states of samples with fluorine were determined experimentally with preservation of relative difference in component bond energies and their intensities in keeping with the calculation in [3] for simple oxides. Full width at half maximum (FWHM) of all the components was ΔE = 1.6 eV. Decomposition was performed by Gauss–Newton method.

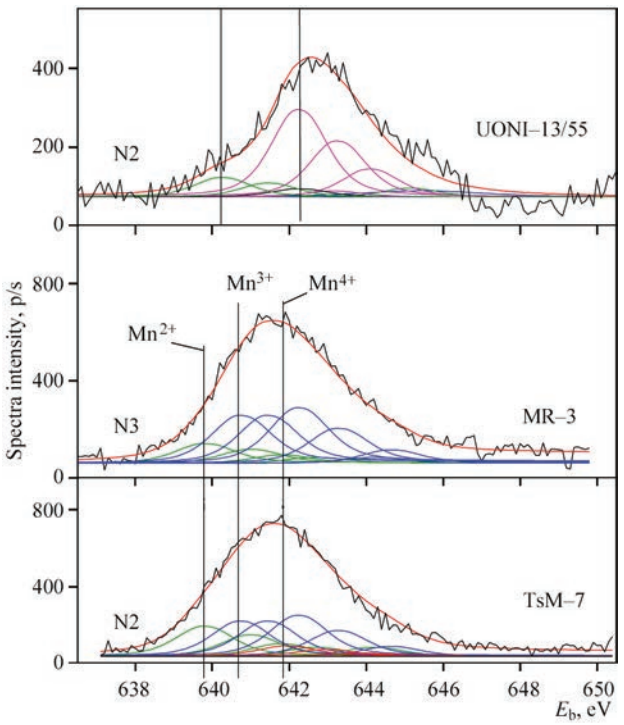

Figure 1. $Mn2p_{3/2}$ spectra of welding aerosol samples decomposed by RFA method into components

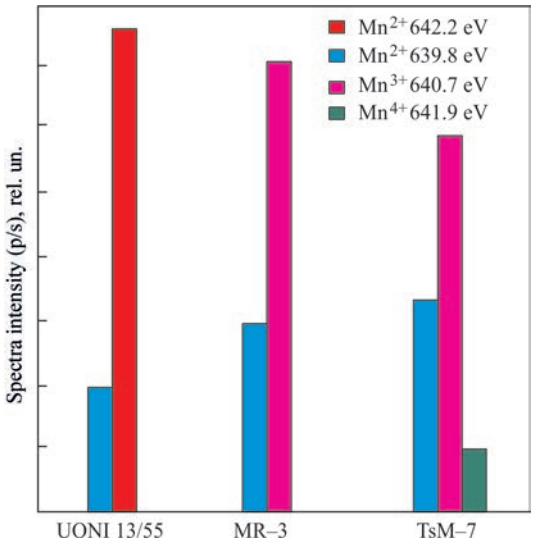

Figure 2. Histograms of relative content of Mn^{2+}, Mn^{3+} and Mn^{+4}-states in $Mn2p_{3/2}$-spectra of the samples

Results and their discussion. For all the components FWHM = 0.85 eV. Mn^{2+}-, Mn^{3+}- and Mn^{4+}-states are modeled by groups of five components, in keeping with the data of work [6]. First components of the groups for $Mn2p_{3/2}$-line have bond energies of 639.75, 640.2 eV, 640.7, 640.7 and 641.9 eV, respectively (Table 1). First component from the group, describing Mn^{2+}-states in Mn-F bond, has E_b 642.1, 642.2 eV [7]. Components, released by *E*, are decomposed into *E*-spectra from Table 1.

By RFS data given in Figures 1, 2 and in Table 2, one can see that the relative intensities between Mn^{2+}-, Mn^{3+}- and Mn^{4+}-states in the spectra of UONI 13/55 samples and MR-3 samples are essentially different that allows sorting them into two separate groups.

Table 3 presents the results of X-ray fluorescent analysis of the composition of SCWA forming in coated-electrode welding.

UONI 13/55 sample features greater CaO content (Table 3) that is related to presence of marble in the electrode coating. In this sample, where iron exists in the composition of ferromanganese, ferrosilicium and ferrotitanium, the content of Mn^{2+}-states, which can be associated with iron spinels, decreases. Instead, the content of Mn^{2+}-states, corresponding to Mn-F bond in MnF_2, rises in the spectra. The fixed absence of oxide phases with Mn^{3+}- and Mn^{4+}-states is attributable to the reducing action of fluorine and fluorine competition. Almost the same ratio of Mn^{2+}- and Mn^{3+}-states was registered in MR-3 samples. A feature of

Table 2. Relative contributions of Mn^{2+}, Mn^{3+} and Mn^{+3}-components (%) in $Mn2p_{3/2}$-spectra in samples 1-5

Sample name/bond	Mn^{2+}–O 640.2	Mn^{2+}–F 642.2	Mn^{2+}–O 639.75	Mn^{3+}–O 640.70	Mn^{4+}–O 641.9
UONI-13/55	22.6	77.4	–	–	–
MR-3	–	–	29.5	70.5	–
TsM-7	–	–	32.4	58.5	9.1

Table 3. SCWA composition in coated electrode welding, wt.%

SCWA components	Coating type			
	UONI-13/55	MR-3	ANO-36	TsM-7
SiO_2	6.92	19.94	26.0	18.5
TiO_2	0.44	2.18	1.92	0.055
Fe_2O_3	25.89	38.50	34.31	31.78
MnO	5.20	7.15	6.59	15.90
CaO	16.16	022	0.202	0.108
K_2O	10.12	12.92	14.12	7.93
Na_2O	25.2	13.06	7.1	15.9

the spectrum of TsM-7 sample is the contribution of Mn^{4+}-states in Mn-O bond. The coating of TsM-7 electrodes, has the greatest absolute content of manganese and the smallest content of titanium, calcium and potassium (Table 3).

In keeping with literature data, no Mn^{4+}-states were detected, when studying the welding aerosols by RFA method [7–9]. In these works, however, $Mn2p_{3/2}$ spectra were either not decomposed into components, or were decomposed without allowing for the satellite structure of the lines. Presence of Mn^{4+}-states in the aerosols is difficult to register by AES method [6], because of greater width of the lines, as a result of multielectron processes. Application of RFS method when allowing for the satellite components allowed registering Mn^{4+}-state contribution in TSM-7 sample.

Conclusions

Performed work showed that in aerosol samples produced in welding with TsM-7 electrodes, the RFS method realized in electron spectrometer with energy analyzer PHOIBOS-100 SPECS, can be recommended for studying manganese content in Mn^{4+} in welding aerosol.

1. Pokhodnya, I.K., Gorpenyuk, V.N., Milichenko, S.S. et al. (1990) *Metallurgy of arc welding. Processes in arc and melting of electrodes.* Ed. by I.K. Pokhodnya. Kiev, Naukova Dumka [in Russian].
2. Grishagin, V.M. (2011) *Welding aerosol: Formation, examination, localization, application.* Tomsk, TPU [in Russian].
3. Qiang, Zhen, Ruifang, Chen, Kai, Van, Rong, Li (2007) Synthesis of ZrO_2–HfO_2–Y_2O_3–Sc_2O_3 nano-particles by sol-gel technique in aqueous solution of alcohol. *J. of Rare Earths*, 25(**2**), 199–203.
4. Briggs, D., Seach, M.P. (1983) *Practical surface analysis by Auger and X-ray photoelectron spectroscopy*, John Wiley & Sons, Chichester – New York.
5. Diagne, C., Idriss, H., Pearson, K.et al. (2004) Effi cient hydrogen production by ethanol reforming over Rh catalysts. Effect of addition of Zr on CeO_2 for the oxidation of CO to CO_2. *Comptes Rendus Chimie*, 7(**6**), 617–622.
6. Foschini, C.R., Souza, D.P.F., Paulin Filho, P.I., Varela, J.A. (2001) AC impedance study of Ni, Fe, Cu, Mn doped ceria stabilized zirconia ceramics. *J. Eur. Cer. Soc.*, 21(**9**), 1143–1149.
7. Yanmei, Kan, Guojun, Zhang, Peiling, Wang et al. (2006) Yb2O3 and Y2O3 co-doped zirconia ceramics. *Ibid.*, 26(**16**), 3607–3612.
8. Markaryan, G.L., Ikryannikova, L.N., Muravieva, G.P. et. al. (1999) Red-ox properties and phase composition of CeO_2–ZrO_2 and Y_2O_3–CeO_2–ZrO_2 solid solutions. *Colloids and Surfaces A: Physicochemical and Engineering Aspects*, 151(**3**), 435.
9. Marrero-López, D., Peña-Martínez, J., Ruiz-Morales, J.C. et al. (2008) Phase stability and ionic conductivity in substituted La2W2O9. *Bol. Soc. Esp. Ceram. V.*, 47(**4**), 213–218.

Received 15.03.2021

JUNE 12, 1944 The fascist Germany began bombing of London and other British cities with V-1 flying bombs «V-1». Their mass production during the World War II became possible due to the application of welding, with the help of which the spherical cylinders for compressed air, required for engine operation, were manufactured. The fairing and body lining were made of aluminum alloys. The structures of fuselage, wings, stabilizer and other assemblies were manufactured of low-carbon steel using spot welding, mainly with hand tongs.

JUNE 13, 1901 In the middle of 1901, the first acetylene-oxygen welding torch was designed by French engineers Edmond Fouche and Charles Picard. Its design has not fundamentally changed until nowadays. The development of acetylene generators led to an increase in their reliability, and in 1960, the industrial application of this type of welding in the construction of gas pipelines, technological equipment and other structures began.

JUNE 14, 1952 The construction of USS Nautilus (SSN-571), the first in the world nuclear-powered submarine, began. It was adopted by the US Navy on September 30, 1954. On August 3, 1958 «Nautilus» reached the North Pole and became the first ship in the history of mankind, which passed this point of the Earth on its own power. In the United States, to manufacture the first nuclear-powered submarine «Nautilus» the company «General Dynamics» used different joining technologies, mainly submerged arc welding and oxyacetylene welding.

JUNE 20, 1939 The first ever flight of German jet aircraft «Heinkel He 176» was performed. This is the first aircraft in the world, driven by a fluid-fuelled jet engine. In the design of the aircraft the welding was widely used. In the course of the works, it turned out that in welding of wing structures the serious technological problems appear. Then, a different wing was designed and manufactured, made by the usual scheme with two longerons, and welding at the critical place was decided to be removed. The wing consoles with an area of only 5.4 m^2 and a span of 5 m had a very high load, being almost 300 kg/m^2 at 1620 kg take-off weight.